Wang *et al. Biochar* (2026) 8:90
https://doi.org/10.1007/s42773-026-00608-w

Biochar

ORIGINAL RESEARCH Open Access

Redistribution of soil mercury species mediated by thiolated biochar under dry–wet cycles

Zongwu Wang[1†], Leiyi Zhang[3†], Hao Hu[1], Jianyi He[4], Zehang Liang[4] and Yao Huang[2*]

Abstract

Frequent heatwave events increase the frequency of soil dry–wet cycles, accelerating soil weathering and indirectly triggering mercury (Hg) activation risks. Thiol-modified biochar (TMB) has been widely demonstrated as an effective environmental material for immobilizing soil Hg. However, whether TMB can maintain long-term stability under frequent dry–wet conditions, and how it regulates key soil components to influence Hg behavior, remain unknown. In this study, 30 cycles of simulated dry–wet alternation confirm that TMB promotes soil mineral weathering to redistribute Hg species, thereby reducing total Hg leaching under acid rain, lowering Hg bioavailability, and decreasing net methylmercury accumulation. Specifically: (i) TMB accelerates the dissolution of soil calcium carbonate ($CaCO_3$) by 19.1%, reducing the total proportion of exchangeable and carbonate-bound Hg by 89.7%, while increasing soil pH by 8.5% and decreasing zeta potential by 1.7-fold, which favors Hg precipitation and electrostatic adsorption by soil particles; (ii) TMB facilitates the transformation of Fe/Al oxides (e.g., Fe_2O_3, Al_2O_3) into hydroxylated forms with stronger binding capacity (e.g., FeO·OH, $Al(OH)_3$), leading to decreased residual-bound Hg and increased oxide-bound Hg; (iii) TMB enhances the release of soil organic matter (e.g., mineral-associated), which improves Hg complexation capacity and reduces its availability, thereby lowering net methylmercury accumulation. Additionally, TMB increases the relative abundances of Bacillales, Gemmatimonadales, and other taxa in soil microbial community, and enhances the species richness and evenness. This study highlights the critical role of TMB-mediated mineral weathering in promoting Hg redistribution, elucidates the intrinsic mechanism underlying long-term Hg immobilization by TMB under heatwave-accelerated dry–wet conditions, and provides a theoretical basis for the sustainable engineering application of TMB in Hg-contaminated soil remediation.

Highlights

- Heatwave-driven dry–wet cycles raise soil Hg risk; TMB fosters Hg immobilization via mineral weathering
- TMB reduces acid rain Hg leaching, lowers Hg bioavailability via $CaCO_3$ dissolution/pH rise, and decreases methylmercury.
- TMB facilitates Fe/Al oxide hydroxylation (stronger Hg binding) and organic matter release, aiding Hg-soil remediation.

Keywords Thiol-modified biochar, Heatwave, Dry–wet cycles, Mercury species, Soil

†Zongwu Wang and Leiyi Zhang have contribute equally to this work.

*Correspondence:
Yao Huang
yhuang@soil.gd.cn; hyao2013@126.com
Full list of author information is available at the end of the article

Springer

Graphical Abstract

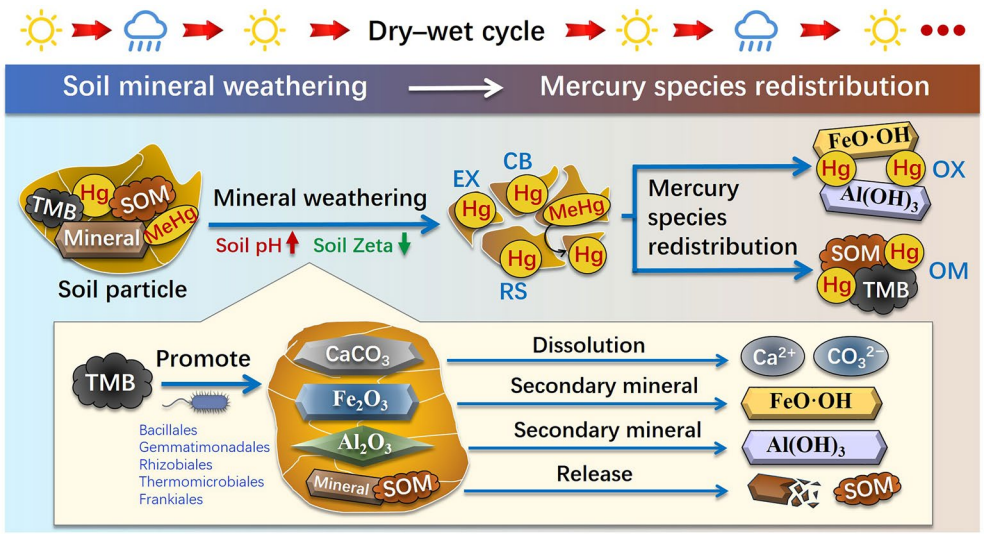

1 Introduction

Mercury (Hg), characterized by high toxicity and persistence, is classified as a priority pollutant worldwide (Chen et al. 2019; Cheng et al. 2025). Owing to its mobility and bioavailability, Hg in soil can contaminate the food chain, harm human health, and threaten ecosystems (Huang et al. 2019a). However, global warming is an ongoing phenomenon, and extreme events (e.g., heatwaves) are occurring with growing frequency (Li et al. 2025; Martinez-Villalobos et al. 2025). Heatwaves accelerate soil weathering, i.e., the alteration of soil mineralogical and chemical composition through processes such as hydration, dissolution, carbonation, hydrolysis, and redox reactions (Jackson and Sherman 1953; Oludare 2017), thereby triggering the risk of soil Hg activation.

Under heatwave conditions, soil moisture dynamics may undergo profound alterations due to strong moisture-temperature coupling, thereby contributing to environmental soil weathering (Li et al. 2025; Maraun et al. 2025; Shao et al. 2025; Zhang et al. 2025). The release of ions (e.g. ions containing N, P, Ca, and Fe) from soil minerals constitutes the initial step, which results in changes to exchangeable cations (Jackson and Sherman 1953; Oludare 2017). This process can alter soil oxidation–reduction potential (ORP) and pH, as well as the mobility, speciation distribution, along with bioaccessibility of soil heavy metals, and the translocation of phosphorus (Conrad et al. 2020; Dixon et al. 2016; He et al. 2026; Meite et al. 2018; Park et al. 2023; Smeck 1973; Zhang et al. 2024; Zhou et al. 2025). Calcium carbonate ($CaCO_3$), a key soil component, can influence metal immobilization via its inherent pH-modulating effect and spontaneous Hg-adsorbing capacity (Breemen et al. 1983; He et al. 2020; Wolthers 2015). Iron oxides and aluminum oxides are widespread forms of Fe and Al in soil, and their forms vary with soil moisture (Fitzpatrick and Schwertmann 1982; Liu et al. 2025). Redox reactions can alter the forms of soil iron, while soil pH can affect the forms of aluminum minerals (Watanabe et al. 2006). Soil organic matter (SOM) is ubiquitous in soils and can directly affect the release and transformation of Hg (Huang et al. 2025; Lindroos et al. 2003; Raulund-Rasmussen et al. 1998). Acid rain can also impact the release of soil Hg (Li et al. 2024; Wang et al. 2024a), and soil phosphorus concentrations can be regulated by weathering intensity (Dzombak and Sheldon 2020).

In recent years, the potential of thiol-modified biochar (TMB) in the immobilization remediation of Hg-contaminated soils has received increasing attention (Xing et al. 2020; Zhao et al. 2020; Zheng et al. 2025). In previous studies, we confirmed that TMB is an effective strategy for remediating mercury-contaminated soil, and revealed its synthesis mechanism and in-situ mercury immobilization mechanism (Huang et al. 2023, 2019b, 2024; Wang et al. 2024b). However, under heatwave-mediated dry–wet alternating scenarios, two critical aspects for the engineering application of TMB remain unknown: the long-term stability of its mercury immobilization

efficiency, and how it influences the redistribution process of mercury species. On the one hand, recent studies have indicated that the mobility and bioavailability of Hg may undergo transformations during dry–wet cycles (Sun et al. 2020; Zhang et al. 2022). On the other hand, the environmental behaviors of key soil components (e.g., soil minerals, SOM, and microbial community structure) may vary with environmental dry–wet alternations, thereby affecting the bound forms of mercury.

This study focused on Hg-contaminated soils that had been treated with TMB for 2 years in our previous work (Huang et al. 2024), and systematically investigated the environmental behaviors of key soil components (e.g., mineral weathering, SOM release, and microbial community structure shifts) and the redistribution of mercury species mediated by TMB under simulated heatwave-accelerated dry–wet cycles. The objective was to verify the real-world environmental applicability of TMB by assessing the long-term stability of immobilized Hg under heatwave-accelerated dry–wet weathering. We conducted a systematic investigation addressing multiple facets of Hg remediation by TMB during dry–wet alternations: mobility and bioavailability of soil mercury, transformation of mercury species, changes in soil mineralogy and SOM, and the potential for mercury release under prolonged acid rain exposure. The specific objectives of this study are fivefold: (1) to investigate leaching of soil mercury and associated components under simulated heatwave-accelerated dry–wet cycles; (2) to reveal the Hg speciation transformation of soil Hg geochemical fractions determined by sequential chemical extraction during dry–wet alternations; (3) to explore soil mercury release under continuous acid rain leaching; (4) to characterize alterations in soil mineral composition and microbial characteristics; (5) to elucidate the mechanism underlying TMB-mediated soil mineral weathering and mercury species redistribution.

2 Materials and methods

2.1 Simulation of heatwave-accelerated dry–wet weathering

To simulate soil weathering under heatwave-accelerated dry–wet cycles after soil Hg remediation, we applied 12 h incubation at 70% water-holding capacity and 12 h oven-drying at 40 °C. This regime mimics natural field wet–dry fluctuations, improving the study's environmental realism. This cycling regimen was repeated 30 times, with soil samples collected after 0, 5, 15, and 30 cycles for subsequent analyses. All samples were freeze-dried, homogenized by grinding, and passed through a 2-mm mesh prior to characterization. The soils utilized in this study were Hg-contaminated soils that were prepared by mixing TMB with soils at 25 ± 2% moisture content, followed by a 2-year incubation (Huang et al. 2024). The TMB employed herein was carbonized from grapefruit peel under anaerobic conditions (Huang et al. 2023). Detailed information on experimental materials, including chemical reagents, quality assurance (QA) and quality control (QC), TMB synthesis protocols, and TMB-treated Hg-contaminated soils is provided in the Supplementary Material (Texts S1-S3). All treatments were conducted in triplicate. Two TMB-amended soils were examined, with TMB addition rates of 0.2% and 0.4%, denoted as 0.2% TMB soil and 0.4% TMB soil, respectively. A non-amended soil without TMB addition served as the control (CK), and was also prepared in triplicate.

2.2 Simulated acid rain and bioavailability leaching tests

Simulated acid rain and bioavailability leaching tests were conducted on TMB-amended soils subjected to dry–wet cycles. A mixed $H_2SO_4 + HNO_3$ solution extraction (mass ratio 2:1, adjusted to pH 3.20 ± 0.05 with deionized water) was used to evaluate mercury mobility under simulated acid rain conditions (HJ/T 299–2007, China). Detailed information regarding H_2SO_4 and HNO_3 is provided in Text S1. In contrast, a 0.01 mol L^{-1} $CaCl_2$ solution was used to extract bioavailable mercury from soil (Huang et al. 2024). For leaching tests, 1.0 g of soil (dry weight) was mixed with 10 mL of extraction solution in a sealed polyethylene centrifuge tube. The mixture was shaken at 40 rpm for 18 ± 2 h or 24 h (25 ± 2 °C). After shaking, the suspension was centrifuged at 4000 rpm for 10 min. The supernatant was then collected, filtered through a 0.45 μm PTFE membrane, and analyzed. The supernatant was analyzed for total mercury (Hg), total iron (Fe), total phosphorus (P), total aluminum (Al), total potassium (K), total nitrogen (N), and dissolved organic carbon (DOC).

2.3 Continuous leaching tests with simulated acid rain

Soil samples collected after 0 and 30 cycles were subjected to a column leaching experiment. The column system employed in this study primarily consisted of five components: an injection pump (PHD/ULTRA, Harvard Apparatus, USA), a column (006EZ-10-25-FF, Omnifit, UK), a syringe, an automatic sample collector, and connecting tubes. The column (total height = 22 cm) comprised four layers arranged from top to bottom: quartz sand (8.7 g, height = 7.7 cm), the soil mixture (2.0 g soil blended with 4.0 g quartz sand, height = 4.5 cm), quartz sand (10.7 g, height = 9.5 cm), and glass wool (0.2 g, height = 0.3 cm) (Figure S1). The total pore volume (PV) of the column (defined as the volume excluding that occupied by soil, quartz sand, and glass wool) was determined to be 6.48 mL. Simulated acid rain was a mixed $H_2SO_4 + HNO_3$ solution (mass ratio 2:1, adjusted to pH

5.60 ± 0.05 with deionized water). The pH of 5.60 ± 0.05 was selected to represent the average rainfall pH in the soil sampling area over the past decade, thereby authentically reflecting actual field acid rain conditions for investigating the long-term stability of Hg immobilization. The volume of simulated acid rain applied was equivalent to the total rainfall over a 10-year period, corresponding to 5750 mm. The simulated acid rain was injected into the column at a constant flow rate of 0.1092 mL min^{-1}, which corresponds to a pore velocity of 0.139 cm min^{-1}. Effluent samples were collected at an interval of 59.34 min, followed by filtration and subsequent analysis. Key parameters analyzed in the effluent included the dynamic concentrations of total Hg, total Al, and DOC, as well as the effluent pH. In this experiment, the effluent masses of Hg/Al/DOC from the remediated soil packed into the fixed-bed column were adopted, and detailed calculations of these values are provided in Text S4.

2.4 Mercury species analysis

To assess the dynamic changes in mercury (Hg) species, five Hg fractions in soil were extracted via the sequential extraction method developed by Tessier et al. (Tessier et al. 1979) (Text S5). These five fractions are defined as follows: exchangeable (EX), carbonate-bound (CB), Fe–Mn oxides-bound (OX), organic matter-bound (OM), and residual (RS). The bioavailability of these Hg fractions follows the order: EX > CB > OX > OM > RS. Specifically, the EX and CB fractions exhibit the highest bioavailability and thus pose a greater risk of inducing secondary soil pollution. In contrast, the OX and OM fractions are classified as potentially bioavailable and are prone to leaching under favorable environmental conditions. The RS fraction is the most stable, as Hg within this fraction is tightly retained in the crystal lattice of soil minerals. The Risk Assessment Code (RAC) is widely employed to evaluate the ecological risk of Hg in soil (Huang et al. 2019a, 2024). Notably, RAC analysis relies on the fractional results obtained from the Tessier sequential extraction method. Comprehensive details regarding the RAC calculation and evaluation criteria are presented in Text S6.

2.5 Total mercury and methylmercury analysis

The total mercury (Hg) in soil samples was extracted, followed by filtration of the extract. The Hg concentration in the resulting filtrate was determined using an atomic fluorescence spectrometer (AFS) (BAF-4000, Baode, China) (HJ 694–2014). For the analysis of total methylmercury (MeHg) in soil, the $CuSO_4$-HNO_3-CH_2Cl_2 extraction method was employed. After extraction and subsequent filtration, the MeHg concentration in the filtrate was measured via Gas Chromatography-Cold Vapor Atomic Fluorescence Spectrometry (GC-CVAFS) (Brooks Rand model III, Seattle, USA) (Huang et al. 2024).

2.6 Soil properties, mineralogical composition, and microbial characteristics

Soil samples collected after 0 and 30 cycles were freeze-dried prior to further analysis and characterization. The concentrations of total iron (Fe), total aluminum (Al), total potassium (K), and total phosphorus (P) in the samples were determined using an inductively coupled plasma optical emission spectrometer (ICP-OES) (PlasmaQuantPQ 9000, Analytik Jena, Germany) (HJ 776-2015). Dissolved organic carbon (DOC) and total nitrogen (N) contents were measured with a total organic carbon (TOC) analyzer (TOC-LCPH, Shimadzu, Japan). Soil pH was determined using a pH meter (FE28-Standard, Mettler Toledo, Switzerland). The soil zeta potential was analyzed via a nanoparticle zeta potential and size analyzer (Nanotrac wave II, Microtrac, USA). Additionally, the soil mineral composition was characterized by X-ray powder diffraction (XRD) (D8-AXS, Bruker, Germany). To analyze the changes in microbial community structure, total soil DNA was extracted using the PowerSoil® DNA Isolation Kit (MO BIO Laboratories, Inc., Carlsbad, CA, USA) following the manufacturer's instructions. The V3-V4 hypervariable region of bacterial 16S rRNA was amplified using 3338F and 806R primers, followed by high-throughput sequencing on the Illumina MiSeq platform. In the true terminal restriction fragments, the relative abundance was calculated as the ratio of the respective peak areas under a given T-RFLP pattern to evaluate bacterial community compositions. Alpha-diversity (α-diversity: Chao1, Simpson, Shannon and Goods_coverage indices) and beta-diversity (β-diversity) analyses were subsequently conducted.

3 Results and discussion

3.1 Mercury and multi-elements leaching behavior under dry–wet alternations

The leaching behavior of mercury and associated components in soil under simulated heatwave-accelerated dry–wet cycles was investigated, with a specific focus on analyzing the mobility and bioavailability of soil Hg. The mobility of soil Hg was evaluated using a mixed $H_2SO_4 + HNO_3$ extractant. Over the 0–30 dry–wet cycles, leachable total Hg concentrations decreased by 82.3% (from 0.096 mg kg^{-1} to 0.017 mg kg^{-1}) in 0.4% TMB soil and by 53.5% (from 1.865 mg kg^{-1} to 0.868 mg kg^{-1}) in 0.2% TMB soil, but only by 7.1% (from 23.663 mg kg^{-1} to 20.993 mg kg^{-1}) in the CK (Fig. 1a). These results indicate that TMB can promote the immobilization of soil Hg under dry–wet alternation. The possible reasons are as follows. First, the elevated soil alkalinity induced by

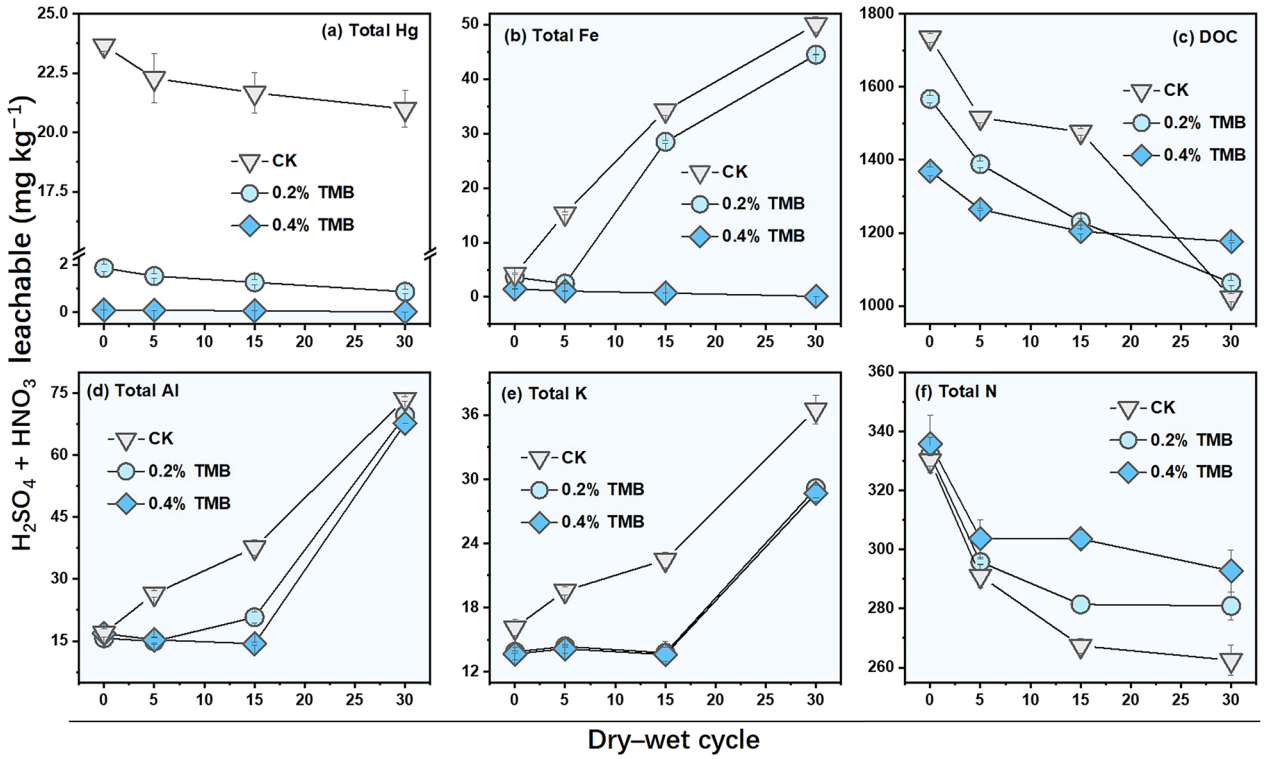

Fig. 1 $H_2SO_4 + HNO_3$ leachable (**a**) total Hg, (**b**) total Fe, (**c**) DOC, (**d**) total Al, (**e**) total K, and (**f**) total N during 0–30 dry–wet cycles. TMB: abbreviation for thiol-modified biochar used in this study. The identical caption applies to all subsequent figures

TMB and dry–wet weathering promotes the formation of $Hg(OH)_2$ and insoluble Fe-bearing phases (e.g., $Fe(OH)_3$) (Fig. 3h), thereby enhancing Hg adsorption onto soil particles through co-precipitation (Breemen et al. 1983). Second, compared with the CK, the zeta potential of the 0.4% TMB soil decreased by 1.7-fold (from −8.33 mV to −22.78 mV) (Fig. S2a). The increased soil electronegativity further enhanced Hg immobilization via stronger electrostatic interactions. Third, with ongoing soil weathering, increasing concentrations of Ca^{2+} and CO_3^{2-} are released, thereby promoting $CaCO_3$ dissolution (Fig. S2b) (Wolthers 2015). Specifically, the content of soluble Ca in 0.4% soil after 15 dry–wet cycles increased by 19.1% (from 311.38 mg kg^{-1} to 370.99 mg kg^{-1}) compared with the CK. This process increases the concentration of free Ca^{2+} in soil (ions with strong ion-exchange capacity for Hg) (Fig. S2b) and further elevates soil pH (Fig. 3h). It can be observed that the soil pH in 0.4% TMB soil after 30 dry–wet cycles increased by 8.5% (from 7.52 to 8.16) compared with the CK. All these changes in soil properties facilitate Hg immobilization. In addition, $CaCO_3$ dissolution can induce the remobilization of substantial Hg originally sequestered in insoluble mineral phases. Given the strong Hg-binding affinity of both TMB and soil organic matter (SOM) (Wang et al. 2024b), the released Hg is rapidly immobilized by the abundant TMB and weathering-derived SOM (Liu et al. 2022). This sequential process facilitates the transformation of Hg from carbonate-bound (CB) fractions to organic matter-bound (OM) fractions, thereby also enhancing Hg stabilization.

As for leachable total Fe, concentrations decreased by 91.8% (from 1.46 mg kg^{-1} to 0.12 mg kg^{-1}) in 0.4% TMB soil during dry-wet cycles, but increased markedly from 3.63 mg kg^{-1} to 44.5 mg kg^{-1} in 0.2% TMB soil and from 4.22 mg kg^{-1} to 50.0 mg kg^{-1} in the CK (Fig. 1b). The underlying mechanisms can be explained as follows: During soil dry–wet weathering, elevated levels of dissolved Fe and dissolved P (e.g., phosphate ions, PO_4^{3-}) are released. Both Hg ions and Fe ions can form precipitates with PO_4^{3-}, with solubility constants of $Ksp(Hg_3(PO_4)_2) = 1.0 \times 10^{-52}$ and $Ksp(FePO_4) = 1.3 \times 10^{-22}$). In 0.4% TMB soil, Hg is predominantly bound to TMB, leaving sufficient PO_4^{3-} to precipitate with dissolved Fe, thus resulting in low leachable total Fe and P (Figs. 1b and S3a). In 0.2% TMB soil, part of the Hg is sequestered by TMB, while the remainder competes for PO_4^{3-}. This reduces the amount of PO_4^{3-} available for Fe precipitation, leading to higher and gradually increasing leachable Fe. In CK, most Hg

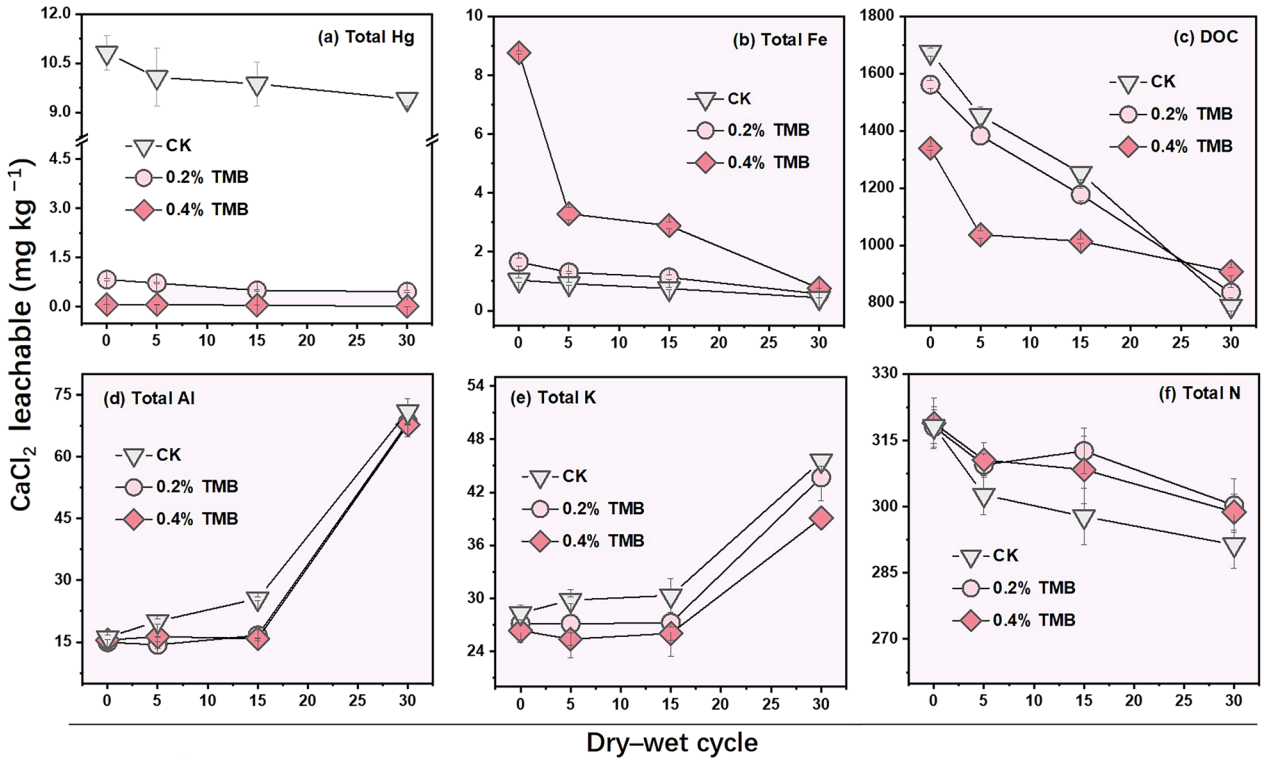

Fig. 2 $CaCl_2$ leachable (**a**) total Hg, (**b**) total Fe, (**c**) DOC, (**d**) total Al, (**e**) total K, and (**f**) total N during 0–30 dry–wet cycles

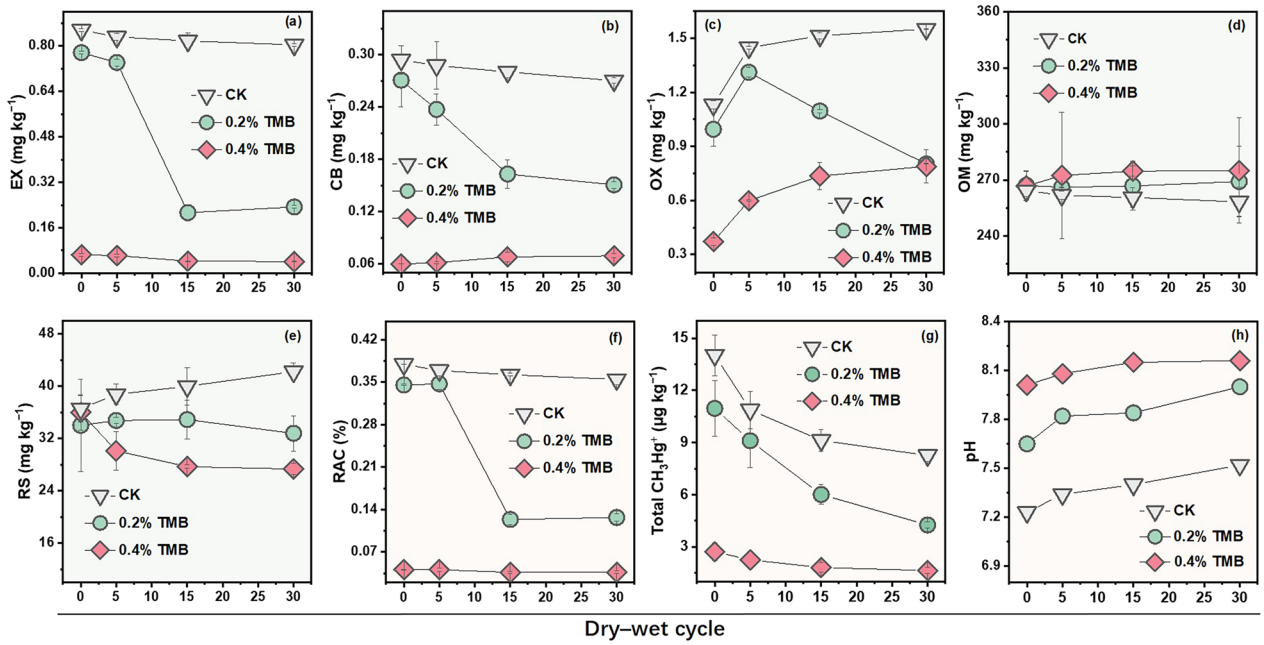

Fig. 3 Mercury speciation dynamics over 0–30 dry–wet cycles: (**a**) exchangeable (EX), (**b**) carbonate-bound (CB), (**c**) Fe–Mn oxides-bound (OX), (**d**) organic material-bound (OM), (**e**) residual (RS), (**f**) RAC, (**g**) total methylmercury (MeHg); (**h**) soil pH over 0–30 dry–wet cycles

binds preferentially with PO_4^{3-}, leaving almost no PO_4^{3-} available to precipitate Fe. As a result, leachable total Fe increase sharply and reach significantly higher levels. The dynamics of leachable DOC (representing released SOM) during dry–wet cycles generally match those of leachable total Hg (Fig. 1c). This correspondence can be ascribed to the strong affinity of Hg for complexation with organic ligands. With increasing dry–wet cycles, both leachable total Al and leachable total K increased significantly (Fig. 1d, e). This can be attributed to enhanced soil mineral weathering under repeated dry–wet cycles, which transforms initially insoluble minerals into soluble species, thereby promoting the release of Al and K. Furthermore, TMB inhibited the release of leachable Al and K ions, which may be attributed to the cation adsorption capacity of TMB itself. As far as total leachable N is concerned, TMB significantly enhanced N immobilization (Fig. 1f). This could be attributed to TMB-stimulated soil microbial activity, which further promotes microbial N immobilization (Lehmann et al. 2011).

The bioavailability of soil Hg was determined using $CaCl_2$ solution as extractant. Under simulated dry–wet cycling, TMB facilitated the reduction of bioavailable Hg in soil, a trend consistent with that of leachable Hg (Figs. 1a and 2a). This mechanism is consistent with that discussed above. Compared with concentrations extracted by the mixed $H_2SO_4+HNO_3$ solution, those of labile total Fe and labile total P extracted by $CaCl_2$ solution were significantly lower (Figs. 2b and S3b). For example, Fe existed mainly in amorphous FeO·OH phases, largely because the $CaCl_2$ extractant lacks strong dissolving capacity, unlike strong acids. The variation patterns of bioavailable DOC, total Al, total K, and total N were consistent with those obtained using the mixed $H_2SO_4+HNO_3$ solution as extractant (Fig. 2c–f).

In summary, under the mediation of TMB, the mobility and bioavailability of Hg in soil showed strong resistance to dry–wet cycles, confirming the long-term stability of Hg immobilization in soil under repeated dry–wet alternations.

3.2 Mercury speciation dynamics under dry–wet alternations

Dynamic variations in mercury fractions were characterized using a sequential extraction procedure. Figure 3a–e illustrates the Hg speciation in soil across 0–30 dry–wet cycles. Relative to the CK and 0.2% TMB treatments, both the EX and the CB fractions in the 0.4% TMB soil remained at low levels (Fig. 3a, b), and the total proportion of exchangeable and carbonate-bound Hg in 0.4% TMB soil at 30 dry–wet cycles was reduced by 89.7% (from 0.35% to 0.04%) compared with CK (Fig. 3f). This can be mainly attributed to TMB-mediated weathering and decomposition of $CaCO_3$ and subsequent Hg release, as well as the resulting ion exchange (between Hg^{2+} and abundant Ca^{2+}) and organic complexation of Hg. This indicates that TMB effectively reduced the bioavailability of Hg. In addition, in soil treated with 0.4% TMB over 0–30 dry–wet cycles, the decrease in the EX-Hg fraction may be attributed to ion exchange between Hg^{2+} and abundant Ca^{2+}, whereas the slight increase in the CB-Hg fraction can be ascribed to the $CaCO_3$ dissolution during dry–wet weathering (He et al. 2020). With respect to the OX fraction in 0.4% TMB soil, its content remained at a low level compared with the CK. This may be attributed to the enhanced weathering of Fe–Mn oxides caused by TMB during soil weathering. Furthermore, the OX fraction increased from 0 to 30 dry–wet cycles, which is consistent with the reduction in bioavailable Fe (Figs. 2b and 3c). This observation can be ascribed to the enhanced formation of Fe-Hg oxide complexes during the dry–wet cycling process (Qiao et al. 2023).

In 0.4% TMB soil, the OM fraction remained at a higher level than that of CK over 0–30 dry–wet cycles (Fig. 3d), which was consistent with the concentration of leachable DOC (released SOM) with strong Hg-binding capacity (Fig. 1c). This observation can be ascribed to the immobilization of Hg released from recalcitrant insoluble minerals (e.g., RS fraction) by TMB or dissolved SOM via complexation during soil weathering, thereby leading to an increase in the OM fraction and a corresponding decrease in the RS fraction. Compared with the CK, the RS fraction in 0.4% TMB soil at 30 cycles decreased by 35.3% (from 42.24 mg kg^{-1} to 27.33 mg kg^{-1}). Under TMB mediation, Hg speciation shifted from the RS to the OM fraction, and OM-bound Hg remained consistently higher than RS-bound Hg across 0–30 dry–wet cycles. Overall, the OM and RS fractions were quantitatively dominant, which effectively enhances the long-term stability of Hg immobilization (Fig. 3d, e). Moreover, results from the RAC assessment demonstrated that all soils posed negligible environmental risk (RAC < 1%) across the entire dry–wet cycling period, and TMB further contributed to mitigating the associated environmental risks (Fig. 3f). Furthermore, the influence of TMB on the total MeHg content during dry–wet cycles was also investigated. For 0.4% TMB soil, total MeHg remained at a significantly low level compared with the CK (from 14.03 μg kg^{-1} to 8.26 μg kg^{-1}), and decreased from 2.72 μg kg^{-1} to 1.64 μg kg^{-1} over the dry–wet cycles. This supports the conclusion that TMB effectively decreased the total methylmercury (MeHg) concentration and effectively inhibited the net formation of MeHg under dry–wet cycles (Fig. 3g).

Thus, during dry–wet cycles, TMB can drive the redistribution of Hg species in soil, transforming Hg from highly bioavailable species (EX, CB) to less bioavailable species (OX and OM), thereby favoring the mitigation of ecological and environmental risks.

3.3 Mercury release during continuous simulated acid rain leaching

The effluent concentrations of total Hg and its associated components (DOC and total Al), together with effluent pH, were determined using soil column experiments under simulated continuous acid rain leaching

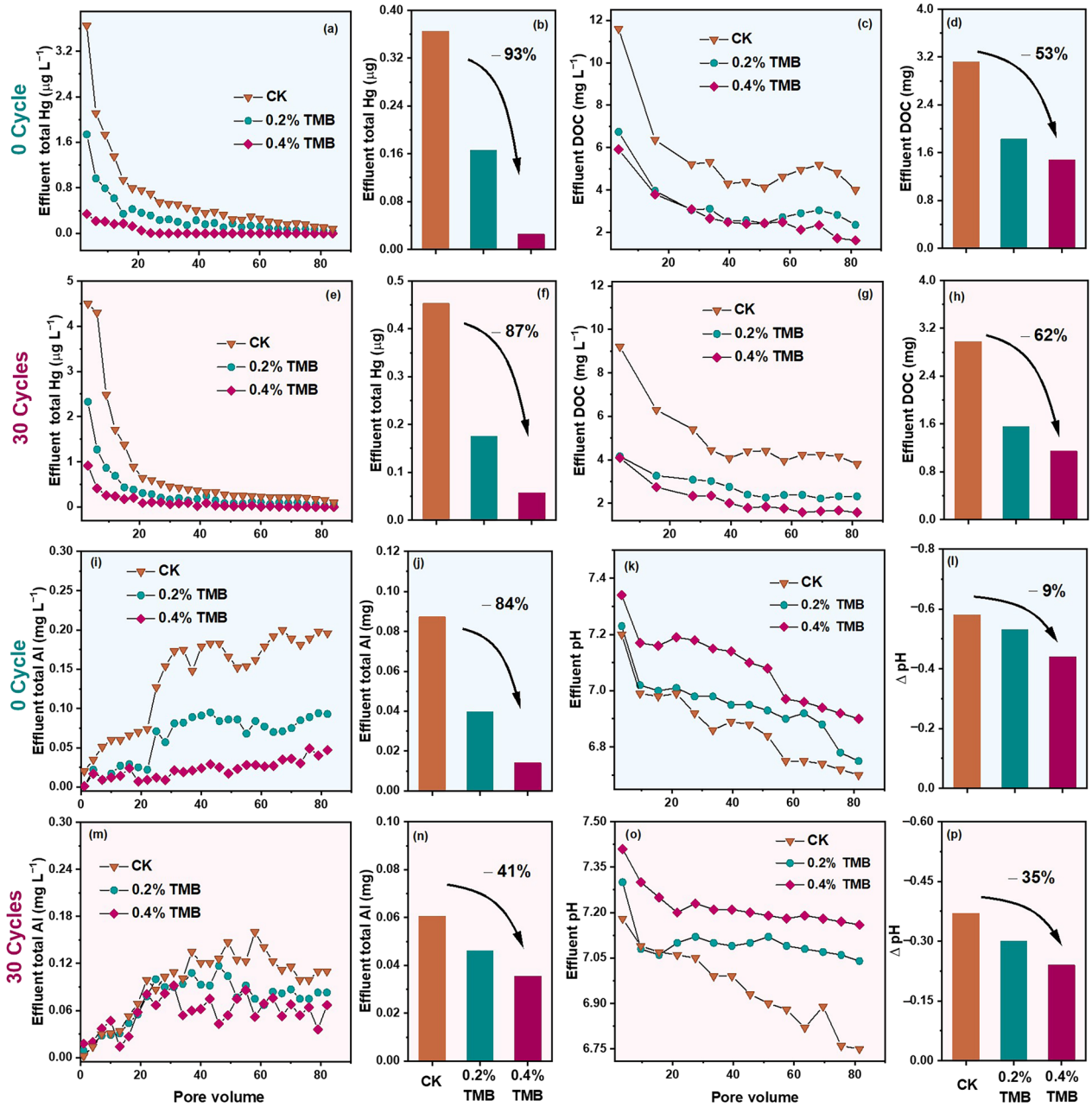

Fig. 4 Continuous simulated acid rain leaching tests. The effluent concentration of (**a**, **e**) total Hg, (**c**, **f**) DOC and (**i**, **m**) total Al after 0 and 30 dry–wet cycles. The effluent mass of (**b**, **f**) total Hg, (**d**, **h**) DOC and (**j**, **n**) total Al after 0 and 30 dry–wet cycles; (**k**, **o**) the effluent pH and (**l**, **p**) the effluent ΔpH after 0 and 30 dry–wet cycles. Effluent total Hg (μg L^{-1}): the instantaneous concentration of Hg in the leachate at each sampling point; the same applies to Al, DOC, and pH. Effluent total Hg (μg): the cumulative mass of total Hg leached from the soil column; the same applies to Al and DOC. ΔpH: the cumulative change in pH between consecutive leachate samples

conditions (Fig. 4). At both 0 and 30 dry–wet cycles, the effluent concentrations of total Hg presented a significant decrease (Fig. 4a, e). In particular, relative to the CK, almost no effluent Hg was detected in 0.4% TMB soil after 27 pore volumes. The total effluent Hg was reduced by 92.9% at 0 cycles (from 0.366 μg to 0.026 μg) and 87.4% at 30 cycles (from 0.454 μg to 0.057 μg) (Fig. 4b, f), demonstrating that TMB remained effective in promoting Hg immobilization even under acid rain leaching conditions. This was partly ascribed to the strong Hg-complexation capacity of TMB and partly to the Hg immobilization ability of DOC, as evidenced by the reduced total effluent DOC (Fig. 4c, d, g, h). The effluent concentrations of DOC exhibited a variation trend identical to that of Hg (Fig. 4c, g). Compared with the CK, the total effluent DOC in 0.4% TMB soil decreased by 52.6% (from 3.12 mg to 1.48 mg) at 0 cycles and by 61.7% (from 2.98 mg to 1.14 mg) at 30 cycles (Fig. 4d, h). This finding further confirms that SOM acts as one of the key contributors to maintaining the long-term stability of soil Hg immobilization. Variations in effluent pH during 0–30 dry–wet cycles are shown in Fig. 4k–l, o–p. At 0 cycles, effluent pH decreased markedly, which could be attributed to elevated total Al in the effluent, together with the hydrolysis of Al and Fe species (Fig. 4i, j, m, n). Specifically, the total effluent Al and Fe likely originated from the dissolution of $Al(OH)_3$ and $FePO_4$, respectively. At 30 cycles, effluent pH in 0.4% TMB soil was comparatively higher; this observation can be ascribed to the inherent alkalinity of TMB and the increased soil alkalinity during dry–wet cycles (Fig. 3h).

3.4 Soil mineral transformations

The mineral compositions of the three soil types at 0 cycle and 30 cycles are shown in Fig. 5. The main compounds in CK and in remediated soil comprised SiO_2 (PDF#38-0360), $CaCO_3$ (PDF#17-0763), $Ca(Mn,Fe)Si_2O_6$ (PDF#33-0292), Fe_2O_3 (PDF#10-1139), $Fe_2O_3{\cdot}H_2O$ (PDF#13-0092), FeO·OH (PDF#44-1415), $(Mg, Fe)_2SiO_4$ (PDF#31-0795), Al_2O_3 (PDF#04-0878), AlO·OH (PDF#48-0890), $Al(OH)_3$ (PDF#38-0376), $CH_5N_3O_3S$ (PDF#37-0510), $FePO_4$ (PDF#31-0647), $Hg_3(PO_4)_2$ (PDF#36-1460), HgS (PDF#19-0798), and HgO (PDF#37-1469).

The soil samples employed in this study were abundant in $CaCO_3$, as confirmed by its characteristic XRD

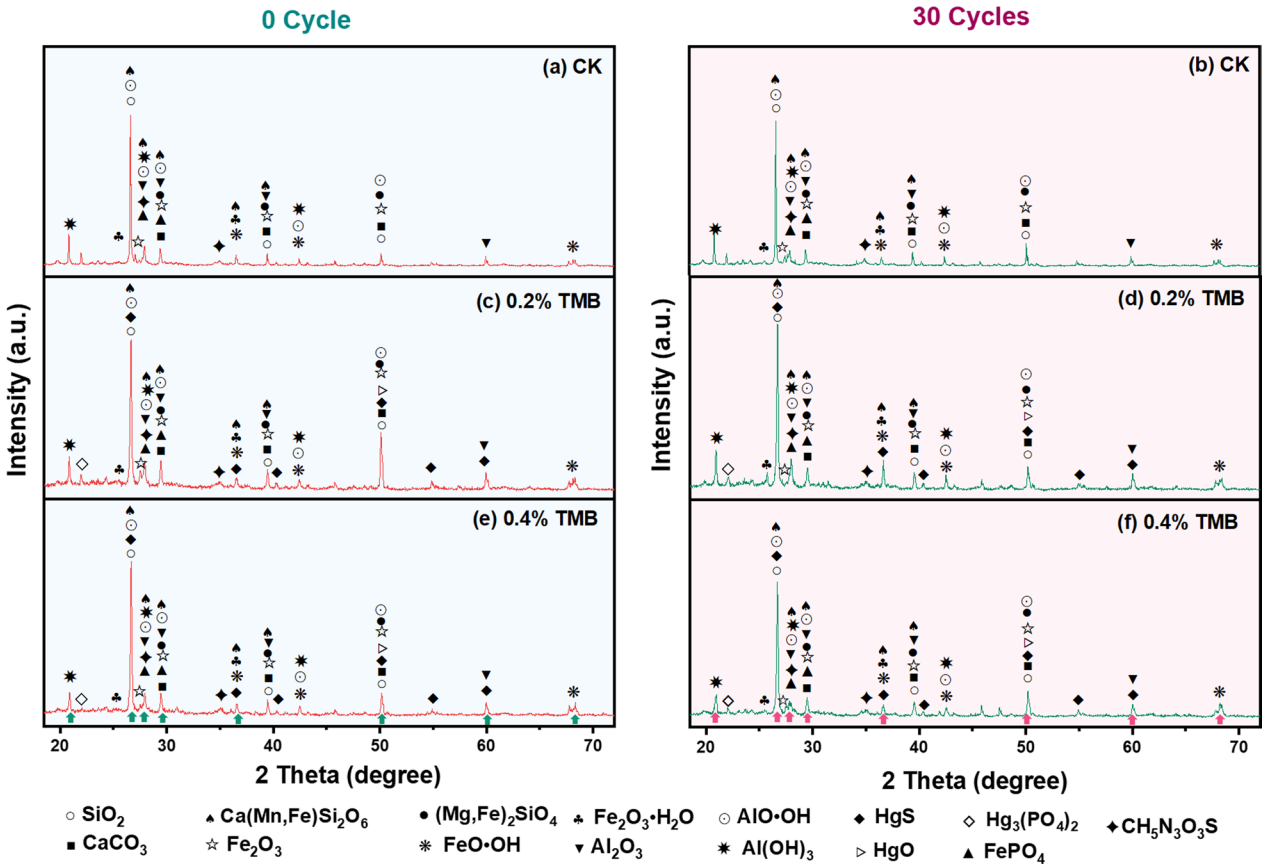

Fig. 5 Mineral composition as affected by TMB after (**a**, **c**, **e**) 0 cycle and (**b**, **d**, **f**) 30 dry–wet cycles

diffraction peaks at 2θ = 21.0°, 29.5°, 39.5°, and 50.4°. At both 0 and 30 dry–wet cycles, the $CaCO_3$ diffraction intensities in 0.4% TMB soil were significantly weaker than those in CK (Fig. 5a, b, e, f). This indicates that TMB enhanced the reduction of soil $CaCO_3$ content during dry–wet cycles, which is attributable to the dissolution of $CaCO_3$ during soil weathering and the consequent acid-neutralization reactions (Breemen et al. 1983; He et al. 2020).

From 0 to 30 dry–wet cycles, compared with CK, the diffraction intensities of stable iron species (e.g., Fe_2O_3, (Mg, Fe)$_2SiO_4$) in 0.4% TMB soil weakened, whereas those of unstable iron species (e.g., FeO·OH, $Fe_2O_3·H_2O$) strengthened. This phenomenon arose from TMB-induced phase transformation of Fe species during soil dry–wet weathering (Jackson and Sherman 1953; Sánchez-Marañón et al. 2023; Watanabe et al. 2006). These changes in Fe species facilitated Hg immobilization, given the strong Hg adsorption capacity of unstable Fe species. Furthermore, unstable Fe species tend to undergo hydrolysis, a process that in turn elevates soil pH. During dry–wet cycling, compared with CK, the diffraction intensities of stable aluminum species (e.g., Al_2O_3, AlO·OH) in 0.4% TMB soil also weakened, whereas those of unstable aluminum species (e.g., $Al(OH)_3$) also strengthened. This could also elevate soil pH, as the hydrolysis of Al species releases OH^- (Fitzpatrick and Schwertmann 1982; Sánchez-Marañón et al. 2023; Watanabe et al. 2006). Therefore, this TMB-mediated hydroxylation of Fe/Al oxide facilitated the transformation of Hg species from residual-bound Hg to oxide-bound Hg. At both 0 and 30 dry–wet cycles, compared to CK, the 0.4% TMB soil exhibited enhanced diffraction intensities of $FePO_4$ and HgS, accompanied by weakened intensities for $Hg_3(PO_4)_2$ (Fig. 5e, f). This occurred because, under sufficient TMB conditions, Hg preferentially interacted with TMB to form stable complexes, leaving PO_4^{3-} available only to bind with Fe.

3.5 Changes in microbial community structure and diversity

The soil microbial community structure and species diversity are presented in Fig. 6. These results demonstrate that TMB effectively reshaped the soil microbial community composition and improved species richness and evenness. Specifically, the relative abundance of dominant bacterial orders is shown in Fig. 6a. This plot reveals significant shifts in community composition mediated by TMB, characterized by the enrichment of Bacillales, Gemmatimonadales, Rhizobiales, Thermomicrobiales, and Frankiales, whereas the relative abundances of Corynebacteriales, Propionibacteriales, Sphingomonadales, and Micrococcales was reduced. No pronounced dose-dependent differences were observed between the 0.2% and 0.4% TMB soils (Huang et al. 2025). Hierarchical clustering analysis at the genus level revealed distinct microbial community structures between the treated groups and the CK (Fig. 6b). The CK formed a separate cluster, characterized by a highly skewed community dominated by *Rhodococcus*. In contrast, TMB-amended soils clustered closely together, indicating similar community profiles, and exhibited a significant reduction in the relative abundances of *Rhodococcus* and a marked enrichment of multiple taxa, including *Bacillus*, *Gemmatiomonas*, *Microvirga*, and *Blastococcus*. This shift led to a more evenly structured microbial community with elevated species richness and evenness, indicating enhanced β-diversity. Negligible differences in community structure were observed between TMB-amended soils. The α-diversity indices calculated based on amplicon sequence variants (ASVs) revealed that TMB mediated substantial shifts in soil microbial communities (Fig. 6c). Compared to CK, 0.4% TMB increased the Chao1 index, indicating enhanced microbial richness. Both 0.2% and 0.4% TMB elevated the Simpson and Shannon indices, reflecting improved community evenness and overall diversity (Fig. 6d–e). Notably, the Goods_coverage index decreased slightly in treated groups but remained close to 1.0, confirming the reliability of the sequencing data (Fig. 6f).

3.6 Proposed mechanisms

TMB sustains the long-term stability of soil Hg immobilization by promoting mineral weathering and Hg species redistribution. Firstly, during dry–wet alternations, TMB facilitates soil mineral weathering and recrystallization (Fig. 7), manifested by $CaCO_3$ dissolution, the formation of Fe/Al hydroxides (e.g., FeO·OH, $Fe_2O_3·H_2O$, $Al(OH)_3$), increased SOM release, and enhanced Hg complexation with soil particles or TMB. Together with favorable TMB-induced changes in soil physicochemical properties (e.g., increased soil pH, reduced zeta potential), these processes collectively strengthen the long-term stability of Hg immobilization. Secondly, TMB-mediated transformation of Hg species during dry–wet cycles reduces Hg bioavailability and environmental risk, with Hg predominantly redistributed into less available fractions (OX and OM). Specifically, TMB facilitates the transformation of Hg from highly available fractions (e.g., EX, CB) to less available forms (e.g., OX and OM), while simultaneously promoting mercury demethylation (Fig. 3). Thirdly, TMB modulates the soil microbial community structure, which is closely consistent with the changes observed in soil microbial community composition and α-diversity (Fig. 6). Specifically, TMB significantly alters the taxonomic composition of soil microorganisms and

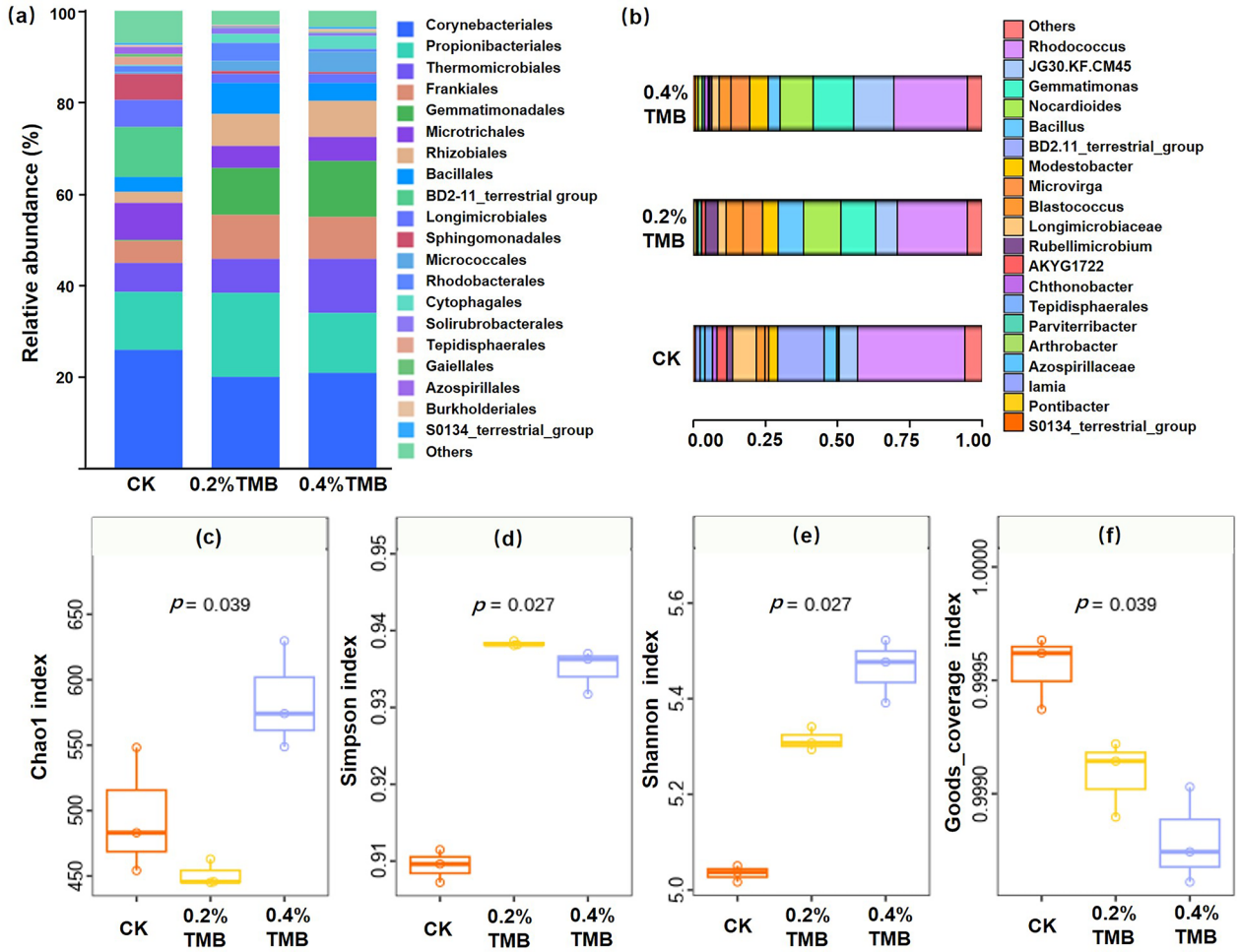

Fig. 6 **a** Microbial community structure at the order level; **b** Hierarchical clustering analysis of β-diversity based on genus-level profiles; **c**–**f** α-diversity indices based on amplicon sequence variants (ASVs) after 30 dry–wet cycles. The p-values are the results of the Kruskal-Wallis test for the three groups (c-f)

enhances α-diversity by increasing species richness and evenness (Fig. 6). These TMB-induced shifts in the soil microbiome may establish a synergistic "functional material–microorganism" system, which could collectively promote the redistribution of Hg species and further contribute to sustaining the long-term stability of Hg immobilization in soil.

4 Conclusions

Through simulating 30 cycles of heatwave-mediated dry–wet alternation, this study systematically revealed the environmental behavior of TMB in promoting mercury species redistribution by mediating soil mineral weathering and SOM release. Specifically, TMB promotes soil mineral weathering, which manifests in multiple interconnected soil property changes: the dissolution of $CaCO_3$, the in-situ formation of Fe/Al hydroxylated forms (e.g., FeO·OH, $Fe_2O_3·H_2O$, and $Al(OH)_3$), a significant increase in soil pH, a reduction in soil zeta potential, and the enhanced release of SOM. Collectively, these TMB-induced soil modifications create a favorable geochemical environment for Hg immobilization. Firstly, mineral weathering releases residual-bound Hg, but the newly formed Fe/Al hydroxides serve as key adsorption sites, facilitating Hg binding to form Fe–Mn oxide-bound Hg. Secondly, both TMB itself and the released SOM function as complexing agents, reacting with Hg to generate organic matter-bound Hg. Moreover, TMB modulates the soil microbial community structure, and significantly alters the taxonomic composition of soil microorganisms and enhances α-diversity by increasing species richness and evenness. These TMB-induced shifts in the soil microbiome may establish a synergistic "functional material–microorganism" system, which could synergistically reinforce the long-term stability of Hg immobilization.

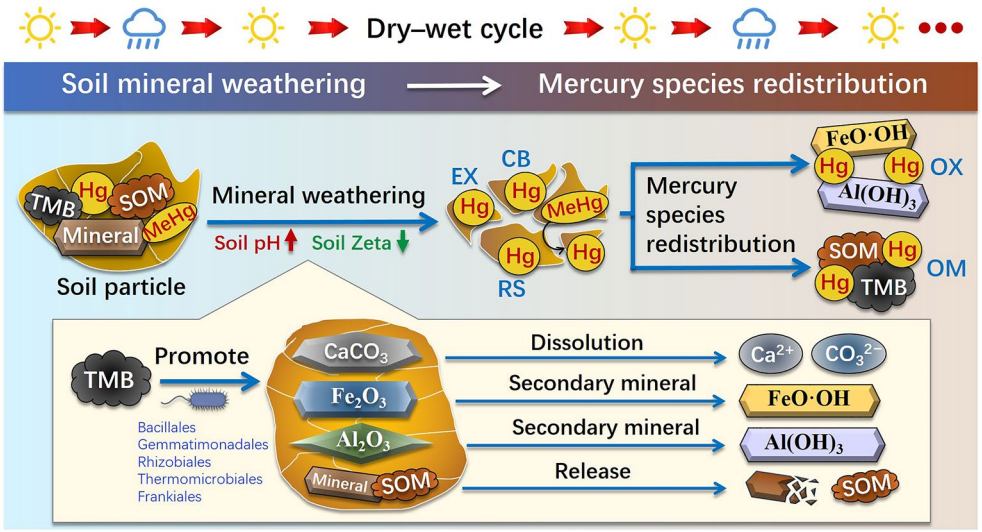

Fig. 7 Proposed mechanisms of TMB-mediated soil mineral weathering and mercury species redistribution. TMB: thiol-modified biochar, SOM: soil organic matter, MeHg: total methylmercury, EX: exchangeable, CB: carbonate-bound, OX: Fe–Mn oxides-bound, OM: organic matter-bound, RS: residual

Together, these two processes drive a critical transformation of Hg species: bioavailable Hg fractions (EX and CB) are converted into stable fractions (OX and OM). This species transformation directly ensures the sustained long-term stability of Hg immobilization in TMB-remediated soil, even under the disturbance of dry–wet alternation. In summary, this study clarifies that TMB promotes soil mineral weathering and Hg species redistribution in soil under dry–wet alternation. The results provide a robust scientific basis for TMB large-scale engineering application with sustainability in Hg-contaminated soil remediation, particularly in regions prone to frequent heatwaves and the associated accelerated dry–wet cycles.

Supplementary Information

The online version contains supplementary material available at https://doi.org/10.1007/s42773-026-00608-w.

Additional file 1.

Funding

This work was supported by the National Natural Science Foundation of China (42577360, 32101397), Major Science and Technology Project of Henan (231100320100), Henan Province Science and Technology Research and Development Plan Joint Funds (232103810037), GDAS' Project of Science and Technology Development (2023GDASZH-2023010103), Guangdong Foundation for Program of Science and Technology Research (2023B1212060044), and Guangzhou Basic and Applied Basic Research Foundation (2024A04J5023).

Author contributions

Zongwu Wang and Leiyi Zhang: Investigation, Data curation, Funding acquisition, Writing—original draft, Writing—review and editing, Resources. Hao Hu: Funding acquisition, Resources, Software, Supervision, Validation. Jianyi He and Zehang Liang: Data curation, Methodology, Software, Visualization. Yao Huang: Conceptualization, Funding acquisition, Formal analysis, Methodology, Project administration, Supervision, Writing—review and editing.

Data availability

All data generated during this study are included in this manuscript and its supplementary information files.

Declarations

Competing interests

The authors declare that they have no known competing financial interests or personal relationships that could have appeared to influence the work reported in this paper.

Author details

[1]Department of Environment Engineering, Yellow River Conservancy Technical University, Kaifeng Engineering Research Center for Municipal Wastewater Treatment, Kaifeng 475004, China. [2]National-Regional Joint Engineering Research Center for Soil Pollution Control and Remediation in South China, Guangdong Key Laboratory of Integrated Agro-Environmental Pollution Control and Management, Institute of Eco-Environmental and Soil Sciences, Guangdong Academy of Sciences, Guangzhou 510650, China. [3]Guangdong Engineering & Technology Research Center for System Control of Livestock and Poultry Breeding Pollution, South China Institute of Environmental Sciences, Ministry of Ecology and Environment of the People's Republic of China, Guangzhou 510535, China. [4]Key Laboratory for Biomass Materials and Energy of Ministry of Education/ Guangdong Provincial Engineering Technology Research Center for Optical Agriculture, College of Materials and Energy, South China Agricultural University, Guangzhou 510642, China.

Received: 28 October 2025 Revised: 21 February 2026 Accepted: 9 March 2026
Published online: 10 April 2026

References

Breemen NV, Mulder J, Driscoll CT (1983) Acidification and alkalinization of soils. Plant Soil 75:283–308. https://doi.org/10.1007/BF02369968

Chen L, Liang S, Liu M, Yi Y, Mi Z, Zhang Y, Li Y, Qi J, Meng J, Tang X, Zhang T, Y. H, Zhang W, Wang X, Shu J, Yang Z (2019) Trans-provincial health impacts of atmospheric mercury emissions in China. Nat Commun 10:1484. https://doi.org/10.1038/s41467-019-09080-6

Cheng P, Li Z, Zheng Y, Meng Q, Yu Y, Jin Y, Gao X, Guo X, Jia L (2025) Study on the regulation of performance and Hg0 removal mechanism of MIL-101(Fe)-derived carbon materials. Sep Purif Technol 379:134939. https://doi.org/10.1016/j.seppur.2025.134939

Conrad SR, Santos IR, White SA, Hessey S, Sanders CJ (2020) Elevated dissolved heavy metal discharge following rainfall downstream of intensive horticulture. Appl Geochem 113:104490. https://doi.org/10.1016/j.apgeochem.2019.104490

Dixon JL, Chadwick OA, Vitousek PM (2016) Climate-driven thresholds for chemical weathering in postglacial soils of New Zealand. J Geophys Res Earth Surf 121:1619–1634. https://doi.org/10.1002/2016JF003864

Dzombak RM, Sheldon ND (2020) Weathering intensity and presence of vegetation are key controls on soil phosphorus concentrations: implications for past and future terrestrial ecosystems. Soil Syst 4:73. https://doi.org/10.3390/soilsystems4040073

Fitzpatrick RW, Schwertmann U (1982) Al-substituted goethite-an indicator of pedogenic and other weathering environments in South Africa. Geoderma 27:335–347. https://doi.org/10.1016/0016-7061(82)90022-2

He G, Zhang Z, Wu X, Cui M, Zhang J, Huang X (2020) Adsorption of heavy metals on soil collected from lixisol of typical karst areas in the presence of $CaCO_3$ and soil clay and their competition behavior. Sustainability Basel 12:7315. https://doi.org/10.3390/su12187315

He J, Huang Y, Mo R, Liang Z, Liang Y, Cui J, Xiao Y (2026) Defect-driven electron transfer for arsenic detoxification in iron-carbon materials. Environ Res 294:123789. https://doi.org/10.1016/j.envres.2026.123789

Huang Y, Wang M, Li Z, Gong Y, Zeng E (2019a) In situ remediation of mercury-contaminated soil using thiol-functionalized graphene oxide/Fe-Mn composite. J Hazard Mater 373:783–790. https://doi.org/10.1016/j.jhazmat.2019.03.132

Huang Y, Xia S, Lyu J, Tang J (2019b) Highly efficient removal of aqueous Hg^{2+} and CH_3Hg^+ by selective modification of biochar with 3-mercaptopropyltrimethoxysilane. Chem Eng J 360:1646–1655. https://doi.org/10.1016/j.cej.2018.10.231

Huang Y, Huang Y, Fang L, Zhao B, Zhang Y, Zhu Y, Wang Z, Wang Q, Li F (2023) Interfacial chemistry of mercury on thiol-modified biochar and its implication for adsorbent engineering. Chem Eng J 454:140310. https://doi.org/10.1016/j.cej.2022.140310

Huang Y, Zhao B, Liu G, Liu K, Dang B, Lyu H, Tang J (2024) Effective reducing the mobility and health risk of mercury in soil under thiol-modified biochar amendment. J Hazard Mater 462:132712. https://doi.org/10.1016/j.jhazmat.2023.132712

Huang Y, Huang Y, Reinfelder JR, Zhong H, Fang L, Liu C, Li F (2025) Phenol-quinone redox couples of natural organic matter promote mercury methylation in paddy soil. Environ Sci Technol 59:1179–1188. https://doi.org/10.1021/acs.est.4c07397

Jackson ML, Sherman GD (1953) Chemical weathering of minerals in soils. Adv Agron 5:219–318. https://doi.org/10.1016/S0065-2113(08)60231-X

Lehmann J, Rillig MC, Thies J, Masiello CA, Hockaday WC, Crowley D (2011) Biochar effects on soil biota—a review. Soil Biol Biochem 43:1812–1836. https://doi.org/10.1016/j.soilbio.2011.04.022

Li W, Deng Y, Wang H, Hu Y, Cheng H (2024) Potential risk, leaching behavior and mechanism of heavy metals from mine tailings under acid rain. Chemosphere 350:140995. https://doi.org/10.1016/j.chemosphere.2023.140995

Li J, Wang S, Zhu J, Wang D, Zhao T (2025) Accelerated shifts from heatwaves to heavy rainfall in a changing climate. Npj Clim Atmos Sci 8:214. https://doi.org/10.1038/s41612-025-01113-w

Lindroos A, Brügger T, Derome J, Derome K (2003) The weathering of mineral soil by natural soil solutions. Water Air Soil Pollut 149:269–279. https://doi.org/10.1023/A:1025684022819

Liu M, Zhu J, Yang X, Fu Q, Hu H, Huang Q (2022) Mineralization of organic matter during the immobilization of heavy metals in polluted soil treated with minerals. Chemosphere 301:134794. https://doi.org/10.1016/j.chemosphere.2022.134794

Liu S, Cen B, Yu Z, Qiu R, Gao T, Long X (2025) The key role of biochar in amending acidic soil: reducing soil acidity and improving soil acid buffering capacity. Biochar 7:52. https://doi.org/10.1007/s42773-025-00432-8

Maraun D, Schiemann R, Ossó A, Jury M (2025) Changes in event soil moisture-temperature coupling can intensify very extreme heat beyond expectations. Nat Commun 16:734. https://doi.org/10.1038/s41467-025-56109-0

Martinez-Villalobos C, Fu D, Loikith PC, Neelin JD (2025) Accelerating increase in the duration of heatwaves under global warming. Nat Geosci 18:716–723. https://doi.org/10.1038/s41561-025-01737-w

Meite F, Alvarez-Zaldívar P, Crochet A, Wiegert C, Payraudeau S, Imfeld G (2018) Impact of rainfall patterns and frequency on the export of pesticides and heavy-metals from agricultural soils. Sci Total Environ 616–617:500–509. https://doi.org/10.1016/j.scitotenv.2017.10.297

Oludare FV (2017) Effects of weathering and erosion on the geochemistry of rocks and soils. Int J Sci Res Sci Technol 3:74–80

Park J, Lee D, Kim H, Woo NC (2023) Effects of dry and heavy rainfall periods on arsenic species and behaviour in the aquatic environment adjacent a mining area in South Korea. J Hazard Mater 441:129968. https://doi.org/10.1016/j.jhazmat.2022.129968

Qiao P, Wang S, Li J, Zhao Q, Wei Y, Lei M, Yang J, Zhang Z (2023) Process, influencing factors, and simulation of the lateral transport of heavy metals in surface runoff in a mining area driven by rainfall: a review. Sci Total Environ 857:159119. https://doi.org/10.1016/j.scitotenv.2022.159119

Raulund-Rasmussen K, Borggaard OK, Hansen HCB, Olsson M (1998) Effect of natural organic soil solutes on weathering rates of soil minerals. Eur J Soil Sci 49:397–406. https://doi.org/10.1046/j.1365-2389.1998.4930397.x

Sánchez-Marañón M, Molinero-García A, Delgado R, García del Moral LF, Martín-García JM (2023) Spectral analysis of Fe oxidation in the early stages of weathering and soil formation. CATENA 222:106850. https://doi.org/10.1016/j.catena.2022.106850

Shao J, Ma H, Song Y, Chen H (2025) Roles of soil moisture-air temperature coupling in three types of heatwaves over the Greater Bay Area of China. J Meteorol Res 39:959–973. https://doi.org/10.1007/s13351-025-4196-0

Smeck NE (1973) Phosphorus: an indicator of pedogenetic weathering processes. Soil Sci 115:199–206. https://doi.org/10.1097/00010694-197303000-00005

Sun Y, Zhang D, Li F, Tao H, Li M, Mao L, Gu Z, Ling Z, Shi H (2020) The rainfall effect onto solidification and stabilization of heavy metal-polluted sediments. R Soc Open Sci 7:192234. https://doi.org/10.1098/rsos.192234

Tessier A, Campbell PGC, Bisson M (1979) Sequential extraction procedure for the speciation of particulate trace metals. Anal Chem 51:844–851. https://doi.org/10.1021/ac50043a017

Wang F, Li W, Wang H, Hu Y, Cheng H (2024a) The leaching behavior of heavy metal from contaminated mining soil: the effect of rainfall conditions and the impact on surrounding agricultural lands. Sci Total Environ 914:169877. https://doi.org/10.1016/j.scitotenv.2024.169877

Wang Z, Jia J, Liu W, Huang S, Chen X, Zhang N, Huang Y (2024b) Mercury speciation transformation mediated by thiolated biochar in high salinity groundwater: interfacial processes, influencing factors, and mechanisms. Chem Eng J 484:149443. https://doi.org/10.1016/j.cej.2024.149443

Watanabe T, Funakawa S, Kosaki T (2006) Clay mineralogy and its relationship to soil solution composition in soils from different weathering environments of humid Asia: Japan, Thailand and Indonesia. Geoderma 136:51–63. https://doi.org/10.1016/j.geoderma.2006.02.001

Wolthers M (2015) How minerals dissolve. Science 349:1288. https://doi.org/10.1126/science.aad0852

Xing Y, Wang J, Shaheen SM, Feng X, Chen Z, Zhang H, Rinklebe J (2020) Mitigation of mercury accumulation in rice using rice hull-derived biochar as soil amendment: a field investigation. J Hazard Mater 388:121747. https://doi.org/10.1016/j.jhazmat.2019.121747

Zhang P, Fan J, Xu X, Xu Z, Yu Y, Zhao L, Qiu H, Cao X (2022) Contrasting effects of dry-wet and freeze-thaw aging on the immobilization of As in As-contaminated soils amended by zero-valent iron-embedded biochar. J Hazard Mater 426:128123. https://doi.org/10.1016/j.jhazmat.2021.128123

Zhang L, Wang B, Wu W, Wang C, Cheng H, Duan X (2024) Enhanced health risk of soil heavy metal exposure following an extreme rainstorm under climate change. Sci Total Environ 954:176409. https://doi.org/10.1016/j.scitotenv.2024.176409

Zhang K, Zuo Z, Mei W, Zhang R, Dai A (2025) A westward shift of heatwave hotspots caused by warming-enhanced land-air coupling. Nat Clim Chang 15:546–553. https://doi.org/10.1038/s41558-025-02302-4

Zhao B, O'Connor D, Shen Z, Tsang DCW, Rinklebe J, Hou D (2020) Sulfur-modified biochar as a soil amendment to stabilize mercury pollution: an accelerated simulation of long-term aging effects. Environ Pollut 264:114687. https://doi.org/10.1016/j.envpol.2020.114687

Zheng Y, Cheng P, Li Z, Fan C, Wen J, Yu Y, Jia L (2025) Efficient removal of gaseous elemental mercury by Fe-UiO-66@BC composite adsorbent: performance evaluation and mechanistic elucidation. Sep Purif Technol 372:133463. https://doi.org/10.1016/j.seppur.2025.133463

Zhou J, Liu Z, Li Z, Xie R, Jiang X, Cheng J, Chen T, Yang X (2025) Heavy metals release in lead-zinc tailings: effects of weathering and acid rain. J Hazard Mater 483:136645. https://doi.org/10.1016/j.jhazmat.2024.136645